Removing surface accretions with piezo-excited high-frequency structural waves

Michał K. Kalkowski*[a] and Timothy P. Waters[a] and Emiliano Rustighi[a]

[a]Institute of Sound and Vibration Research, University of Southampton, Highfield, Southampton SO17 1BJ, United Kingdom

ABSTRACT

Unwanted accretions on structures are a common machinery maintenance problem, which can pose a serious safety threat if not treated effectively and punctually. In this paper we investigate the capability of piezo-excited structural waves for invoking delamination of accreted material from waveguides. We apply a wave-based technique for modelling piezoelectric excitation based on semi-analytical finite elements to model the interface shear stress associated with piezo-actuated structural waves. As a proof of concept, we present a demonstration experiment in which patches of material are removed from a beam-like waveguide with emulated anechoic terminations using ultrasonic excitation.

Keywords: surface accretion removal, ultrasonic de-icing, power ultrasonics, smart structures, structural waves

1. INTRODUCTION

1.1 Motivation

An unwanted material built-up on various types of structures is a common engineering problem in machinery maintenance which seriously affects performance and safety of operation. A type of a potential accretion is defined by the working conditions of a particular object. For aircraft the main problem is the ice accumulation during flight which seriously deteriorates the aerodynamic properties of the wing profile. A similar phenomenon causes wind turbines to experience a drop in efficiency and potentially severely hurt people or damage objects around due to a self-induced ice shedding. Any machinery that works in cold climate regions is often subject to icing issues (e.g. suspension railway, chairlifts, transmission lines). Unwanted accretion is commonly encountered in pipelines. Depositions on their internal walls degrade flow parameters and possibly influence the quality of a transported medium. The last recalled example is ship hull fouling. Hulls suffer from the undesirable accumulation of various types of organisms: algae, plants, microorganisms. The degradation of the properties of the surface is associated with an increase of fuel consumption and requires systematic cleaning and an expensive refurbishment of the hull.

From the aforementioned issues the one that receives the greatest attention from engineers and researchers is aircraft icing. Since the 1920s, when the problem was first noticed, the physics of ice accretion as well as methods of tackling icing have received considerable attention resulting in many anti-/de-icing methods based on various phenomena, of which many are currently in common use. The increased use of composites in modern aircraft has introduced new complications for incorporating standard (especially thermal) methods. Therefore, their drawbacks and limitations are still a challenge to overcome and an inspiration for looking for new ways of neutralising the danger caused by ice accretion.

A potentially promising alternative to the traditional methods for tackling build-ups is a mechanical approach in which the accreted layer is removed with the aid of structural waves induced by piezoelectric actuators. An unwanted build-up is treated as a layer of a multi-layered waveguide. Propagating waves are associated with a frequency dependent stress distribution. Since the bonds created by accretions are usually weaker in shear then in tension, if a high enough shear stress is generated at the interface by a propagating wave the accreted material is debonded.

* e-mail: Michal.Kalkowski@soton.ac.uk

Active and Passive Smart Structures and Integrated Systems 2015, edited by Wei-Hsin Liao, Proc. of SPIE Vol. 9431, 94311T · © 2015 SPIE · CCC code: 0277-786X/15/$18 · doi: 10.1117/12.2087048

1.2 State of the art

The idea of tackling the problem of ice accretion by means of ultrasonic waves was first proposed by Adachi et al.,[1] who noticed that ultrasonic vibration reduces the frost accumulation on a plate excited at a frequency of about 37 kHz (under frosting conditions). The possibility of using guided waves for de-icing has since been spotted and developed in Pennsylvania State University (PSU). The PhD thesis of Ramanathan[2] raised the concept of applying shear horizontal waves as a way of provoking delamination in an iced aluminium plate. Although delamination has been observed during the experiments, thermal processes seem to have played a crucial role in achieving this effect since debonding was not immediate. In parallel, Seppings[3] employed ultrasonic vibration for removing ice and frozen sucrose build-up from pipes.

Palacios (PSU) implemented a 3D finite element model for the preliminary design of the de-icing system and paid particular attention to providing impedance matching for excitation, which lead to very promising experimental results.[4–9] Instantaneous delamination was observed for both freezer and impact ice, proving the feasibility of the method. Palacios' extensive experimental work raised some indications about actuator design and various conditions associated with ice shedding that can facilitate or impede the effect. The follow-up work by Overmeyer et al.[10] addressed various design issues such as the actuators' optimal bonding conditions and techniques to avoid actuator cracking. A successful experimental verification with a few actuators attached to a helicopter blade was also performed.

Zhu (PSU)[11] introduced one possible way of optimising structural design for ultrasonic de-icing purposes which has been named the 'tailored waveguide'. The idea was to make use of the local stress concentration points that occur near the discontinuities within the plate to enhance the generated interface shear stress.

A recent work by DiPlacido et al.[12] (PSU), supported by modelling and experiments, shows that the transient effects associated with switching piezoelectric actuation provide much higher stress than the steady-state response. They also indicate that it is not possible to excite the system continuously at resonance, since the delamination and shedding is very rapid and alters the frequency response of the system during actuation.

Ultrasonic vibration of a plate with frozen water droplets has been recently analysed by Li and Chen.[13] They showed that the droplets can be successfully removed if 60 W of electrical power is supplied to an ultrasonic transducer.

1.3 Outline of the paper

The results presented in the literature to date are very interesting and promising, however there are still some aspects to be developed and investigated. Most of the references recalled above are supported with finite element models representing steady-state ultrasonic vibration. The observed effect is therefore strongly dependent on factors of secondary interest such as dimensions of the plate and boundary conditions. The aforementioned authors refer to wave models to predict stress distributions under free wave propagation, but resort to non-wave based FE models to predict piezo-actuated response. The nature of the interaction of structural waves with unwanted accretions is still not clear and the influence of the boundary conditions cannot be separated from the results achieved.

In this paper we propose an an entirely wave-based approach which can attempt to provide deeper understanding of the conditions promoting delamination associated with propagating waves and insight into power requirements that make this action effective. We apply a wave model for a structure equipped with a piezoelectric actuator to interface shear stress prediction. The model we propose enables including arbitrarily thick actuators with no need for any assumption on its dynamics and supports modelling arbitrary cross-sections (including the bonding layer). As a result, realistic interface shear stress values and electrical power requirements are obtained.

In the final part of the paper we present an experiment on invoking delamination of an accretion from a waveguide with emulated anechoic terminations. The experimental arrangements allowed us to minimise the effect of reflections and demonstrate predominantly the effect of propagating waves. The ultrasonic excitation is shown to be successful in removing surface accretions with power requirements close to those predicted from simulations.

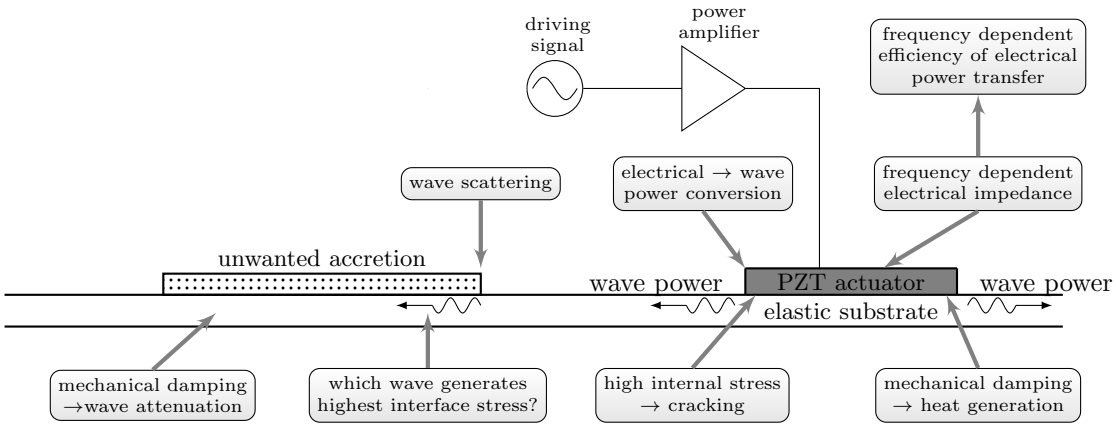

Figure 1: Key aspects of removing surface accretions with piezo-actuated structural waves

In the course of our research we identified a set of critical issues associated with designing an ultrasonic system aimed at delaminating surface accretions. They are listed below in the order of importance and pictured schematically in Fig. 1:

- effective driving of the actuator. The electrical impedance of the actuator bonded to a structure is complex and frequency dependent. Therefore, the actuator can be driven efficiently by an ultrasonic source only at frequencies at which the source and load impedances match. The actuator must be carefully chosen so that the most desirable waves are excited effectively.
- mechanical damping in the actuator at resonance contributes to elevating the temperature. This is undesirable, since the expected effect of ultrasonic action should be achieved instantaneously and by low power mechanical means.
- the actuator driven with high electric field is susceptible to cracking. Appropriate measures need to be adopted.
- it is important to understand the mechanism of converting electrical driving power to propagating wave power to ensure sufficient energy is delivered to waveguide.
- for a particular structure it is useful to understand which wave provides the highest interface shear stress and design the actuation accordingly.
- accretions are often lossy. The waves that carry a large proportion of energy along the accretion are therefore not desirable.

2. WAVE MODEL

The proposed wave-based modelling approach is briefly reviewed in this section. A waveguide with accretion is modelled in the wave domain using semi-analytical finite elements and analytical wave scattering/reflection relationships. The details of the methodology can be found in our previous work[14,15] and only a general introduction is provided here. To assist the description, a schematic workflow is presented in Fig. 2.

The key idea behind the approach is to treat a multi-component one-dimensional waveguide as composed of finite sections of uniform waveguides called wave elements hereafter. In the first step, the structure is subdivided into multiple wave elements. Then, the wave characteristics of each wave element (wavenumbers, wave mode shapes) and excited wave amplitudes (for elements including PZT actuators) are found using the semi-analytical finite element method (SAFE).

The SAFE formulation for mechanical waveguides is well established in the scientific community. It provides the means of obtaining dispersion curves and wave mode shapes by utilising an FE-like procedure for the

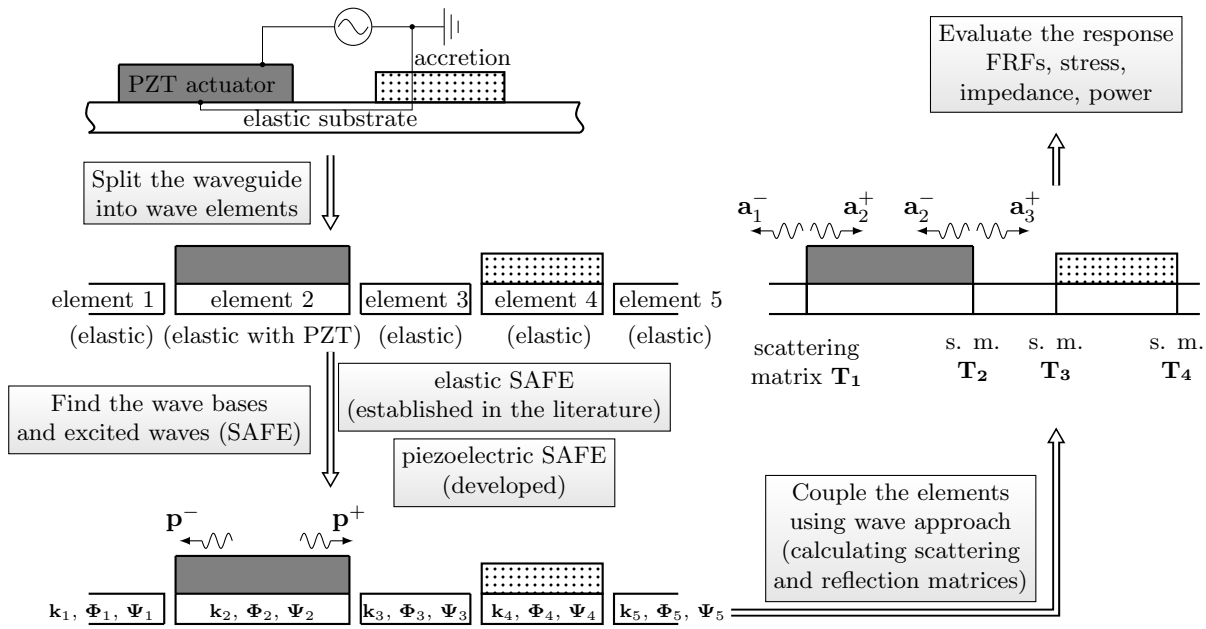

Figure 2: The workflow for calculating the response to the piezoelectric excitation using the modelling approach adopted in the paper.

cross-section discretisation and assuming a harmonic variation of displacement in the waveguide direction.[16–18] Recently the formulation was extended to include materials with piezoelectric coupling enabling the calculation of piezo-excited waves in the wave domain directly with no need for any assumption on the dynamics of the actuator or its mutual interaction with the structure.[14,15] The wave elements are coupled using wave scattering relationships obtained from the wave mode shapes.[19,20] Any desired response is calculated straightforwardly in the final step using matrix algebra.[15]

A vast majority of models for piezoelectric actuation available in the literature originate from the pin-force model,[15,21] for which the actuator is treated as decoupled from the waveguide and represented with an equivalent mechanical traction. For very thin bonding layers, the traction is confined at the ends of the actuator. As both the actuator and its mutual interaction with the structure are modelled as static, these approaches are not well suited for power ultrasonics purposes.

The adopted modelling technique has the following advantages over previously employed methods: firstly, all calculations including piezoelectric excitation are conducted in the wave domain using one model. Secondly, waveguides of an arbitrary cross-section can be considered; this means that we can model a fully three-dimensional scenario assuming that the wave propagates along one direction only (this is not achievable using the pin-force model). Finally, the actuator can be thick and any bonding conditions can be specified – the piezoelectric excitation is modelled directly and the dynamics of both the actuator and the interaction are captured. The model can be formulated in a piece-wise manner[15] which supports an automated calculation of the response of complex multi-component waveguides.

3. WAVE MODEL RESULTS

The capabilities of the adopted modelling approach are presented in this section. To investigate the effect solely of propagating waves, we analyse structures of an infinite extent in the direction of propagation. In particular, we are interested in the interface stress associated with a piezo-actuated wave propagating across in the accretion of the waveguide with reference to the driving voltage and consumed electrical power. The material properties used throughout this paper are gathered in Tab. 1a and Tab. 1b. In the chosen coordinate system z is the propagation direction, y is the thickness direction and x is the width direction.

Property	value
ρ, $\mathrm{kg\,m^{-3}}$	7850
η	0.007
$c^E_{xx} = c^E_{zz}$, GPa	126.35
$c^E_{xy} = c^E_{yz}$, GPa	58.68
c^E_{yy}, GPa	99.88
c^E_{xz}, GPa	62.93
c^E_{xz}, GPa	31.71
$c^E_{yz} = c^E_{xy}$, GPa	36.77
$\varepsilon^\epsilon_{xx} = \varepsilon^\epsilon_{zz}$, $\mathrm{F\,m^{-1}}$	5.5e-09
$\varepsilon^\epsilon_{yy}$, $\mathrm{F\,m^{-1}}$	5.196e-09
$e_{yxx} = e_{yzz}$, $\mathrm{N\,V^{-1}\,m^{-1}}$	-3.239
$e_{zyz} = e_{xyx}$, $\mathrm{N\,V^{-1}\,m^{-1}}$	13.075
e_{yyy}, $\mathrm{N\,V^{-1}\,m^{-1}}$	16.335

(a) Noliac NCE40 PZT ceramics (material used in the experiments).

material	E, GPa	ν	ρ, $\mathrm{kg\,m^{-3}}$	η
aluminium	70	0.3	2700	0.002
steel	163	0.3	8000	0.0001
silvered epoxy	15	0.4	1000	0.0001
glaze ice	8.2	0.351	900	0.01
rime ice	1.5	0.282	600	0.01

(b) Isotropic materials – The properties for ice are chosen within the typical range reported in the literature[6, 22, 23] except the loss factor which is assumed.

Table 1: Material properties used throughout the paper.

For most practical cases (including ice accretion) the bond created by the build-up is weaker in shear than in tension, hence the interface shear stress is responsible for invoking delamination. The aim is therefore to overcome the shear adhesion strength of the added layer. From the three stress components, the transverse shear stresses are expected to contribute to inducing delamination.[6] Given that z is chosen as a propagation direction and y as the thickness direction in this paper, σ_{yz} and σ_{yx} are the components of interest. We confine our attention to σ_{yz} as this stress component is dominant in the considered cases.

3.1 Interface shear stress associated with piezo-actuated structural waves

Firstly, let us look at how different waves contribute to the piezo-induced interface shear stress in structures with unwanted accretions when no reflections are present. To keep both generality and the reference to a practical case, we consider two configurations for the host structure: a 2 mm thick aluminium plate in plane strain (1D cross-section) and a 24×3.42 mm steel rectangular beam (2D cross-section) as used in the experiment presented in the last section of this paper.

We compare the effects of propagating waves only which means that the waves that are classified as evanescent are not taken into account. The loss factor for ice adopted in this paper is high $\eta_{\text{ice}} = 0.01$, so the wave attenuation at high frequencies is expected to be non-negligible. The criterion for identifying propagating waves is in general arbitrary and here it is assumed that propagating waves are associated with the imaginary part of the wavenumber such that $|\mathrm{Im}\{k\}| < 100$.

3.1.1 Infinite plate in plane strain (1D cross-section)

The waveguide and the actuator are modelled under the plane strain assumption, hence only Lamb wave propagation is allowed (i.e. with the motion confined within the y–z plane). The wave composition of the FRF where the interface shear stress is taken as response (called the stress FRF hereafter) is shown in Fig. 3a. The contributions of particular waves are plotted as magnitudes, whereas the total response is the sum of the contributions which accounts for the phase differences. The corresponding phase velocity dispersion curves are plotted in Fig. 3b for reference purposes. Highlighted sections of the dispersion curves in Fig. 3b correspond to a more strict propagation condition, namely $|\mathrm{Im}\{k\}| < 10$. This illustrates how the attenuation in the accreted layer grows with frequency and confirms that the build-up dominated modes decay very quickly.

The pattern of peaks and valleys in the predicted interface stress is mainly related to the relationship between the length of the actuator and the excited wavelength. Peaks also occur close to the cut-off frequencies, at which the deformation of the waveguide is large.

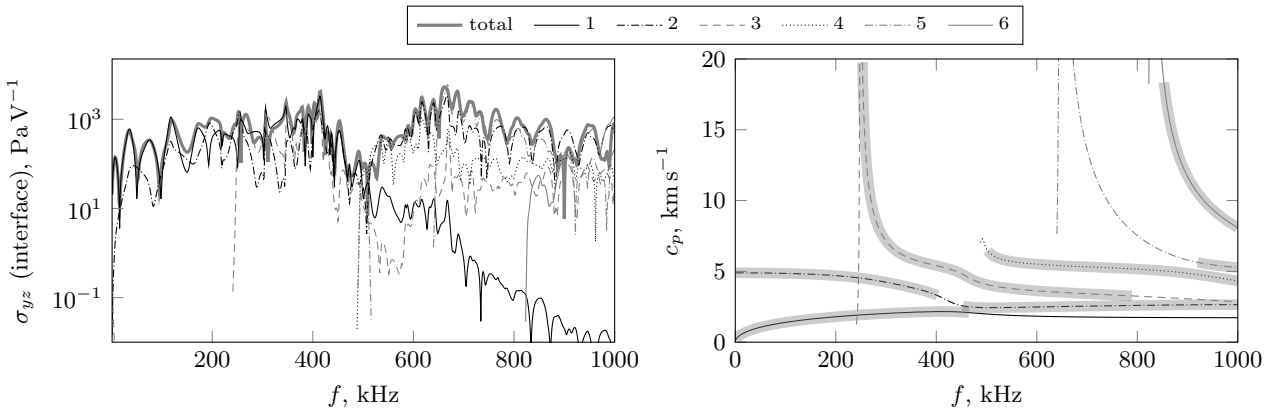

(a) wave contributions to the overall interface shear stress.

(b) phase velocity dispersion curves; highlighted sections of the curves indicate that the condition $|\mathrm{Im}\{k\}| < 10$ is fulfilled.

Figure 3: Interface shear stress and dispersion curves for an infinite aluminium (2 mm) – glaze ice (2 mm) plate in plane strain equipped with a Noliac NCE40 2 mm thick and 5 cm long actuator. Wave mode labelling is the same for both subfigures

Up to ca. 200 kHz the interface shear stress is generated predominantly by the flexural wave (1$^{\mathrm{st}}$ wave, often called A_0). The maximum stress is related to the cut-off frequency of wave 5 at around 660 kHz. Higher-order waves give a significant rise to the interface stress over a narrow bandwidth close to the cut-off frequency. Note that at a longer distance from the actuator the contributions of waves that are not covered by the highlighted sections in Fig. 3b become negligible due to wave decay.

In the frequency range that is expected to be the most practical for wave-induced delamination (wave attenuation grows with frequency), i.e. up to around 200-300 kHz the 1$^{\mathrm{st}}$ wave (flexural – A_0) provides the highest interface shear stress. The stress given by the compressional wave (2$^{\mathrm{nd}}$ – S_0) is significantly lower, particularly below 150 kHz (see Fig. 3a).

3.1.2 Infinite beam-like waveguide as used in the experiment (2D cross-section)

A beam-like waveguide is apparently very similar to the previously considered case, however the associated wave spectrum is much more complex. The waveguide is now finite in the width direction, therefore higher-order modes occur at lower frequencies. Mode tracking becomes a cumbersome task since the wave mode shapes are rather complex and difficult to classify as they change along a dispersion curve significantly.

A representative set of interface shear stress results is presented in Fig. 4a and associated dispersion curves shown in Fig. 4b. At high frequencies the number of waves hinders the analysis of the wave composition of the stress FRF, therefore only a limited frequency range is discussed. The two fundamental and the first higher-order wave are labelled in Fig. 4b to facilitate associating a particular colour with a deformation pattern.

At low frequencies the interface shear stress is generated predominantly by the fundamental flexural wave (1$^{\mathrm{st}}$ in Fig. 4a). The first higher-order wave cuts off at around 30 kHz and from that point prevails in the response. The cut-off of this higher-order wave is associated with a across-width resonance of the cross-section. The global stress peak around 36 kHz is related to the cut-off frequency of the same higher-order wave (across-width bending) in the PZT-covered section. These effects are very notable for the generated interface stress and cannot be captured by simplified models (such as the pin-force model).

The contribution of the wave associated with a longitudinal deformation becomes significant around 80 kHz. Up to 80 kHz only the fundamental flexural wave and the first higher-order wave invoke non-negligible interface shear stress. Note that the maxima of the response are usually related to the cut-off frequencies in the PZT-covered section.

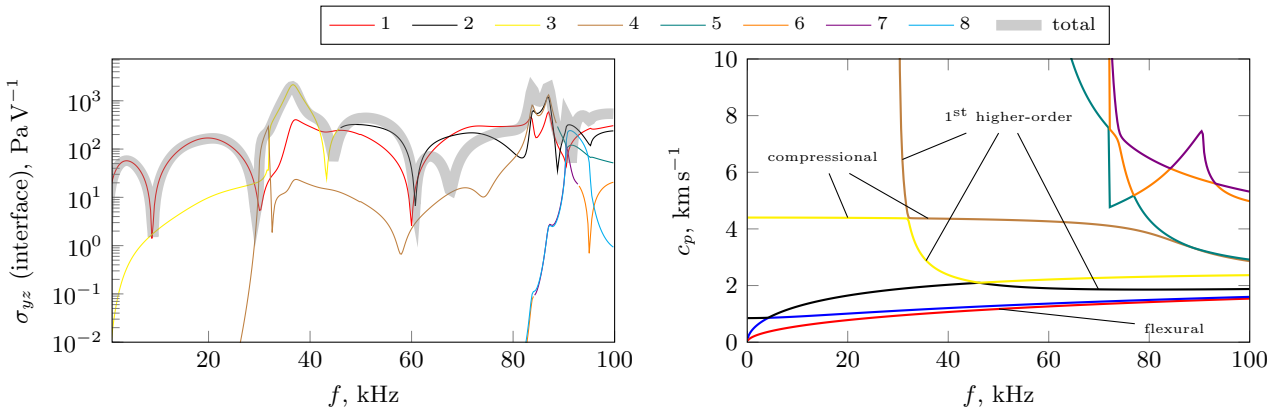

(a) wave contributions to the overall interface shear stress.

(b) phase velocity dispersion curves (real part) for which $|\mathrm{Im}\{k\}| < 100$.

Figure 4: Interface shear stress and dispersion curves for a 24×3.42 mm steel beam covered with 3 mm thick glaze ice accretion equipped with a Noliac NCE40 2.2 mm thick and 7.6 cm long actuator. Wave mode labelling is the same for both subfigures

3.2 Electrical power requirements

A critical quantity describing the applicability of the wave-based ultrasonic de-icing systems is the electrical power requirement. The implemented wave model enables extracting the power consumed by the PZT actuator. However, since the actuator is a complex electrical load the power transfer issues have to be accounted for. The efficiency of the electrical power transfer between an ultrasonic source (amplifier) and a receiver (actuator) depends on the impedances of these elements.

At frequencies of interest the electromagnetic wavelength is very large, hence the system can be well represented by a simple lumped parameter circuit (Fig. 5), where v_S is the voltage of the Thévenin's equivalent voltage source, Z_S is the impedance of the source and Z_L is the impedance of the load. The voltage across the load and the current flowing through it can be calculated as

$$v_L = v_S \frac{Z_L}{Z_L + Z_S} \qquad \text{and} \qquad I = v_S \frac{1}{Z_L + Z_S} \tag{1}$$

The time-average of the power (active) absorbed by the actuator is obtained from

$$P_R = \frac{1}{2}\mathrm{Re}\{v_L I^*\} = \frac{1}{2}\mathrm{Re}\left\{\left(v_S \frac{Z_L}{Z_L + Z_S}\right)\left(v_S \frac{1}{Z_L + Z_S}\right)^*\right\} = \frac{1}{2}|v_S|^2 \frac{\mathrm{Re}\{Z_L\}}{|Z_L + Z_S|^2} \tag{2}$$

Eq. (2) indicates that power transfer is maximum if the impedance of the load is a conjugate of the impedance of the source. This is often not the case for a frequency dependent impedance of the actuator. In order to make the power from Eq. (2) available for the load, the amplifier needs to be capable of delivering $\frac{1}{2}v_S I^* = \frac{1}{2}\frac{|v_S|^2}{Z_L + Z_S}$.

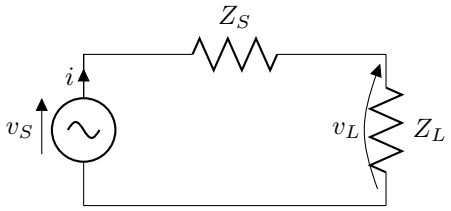

Figure 5: Lumped parameter circuit representing the power source–actuator system.

As for complex loads, the power rating of the amplifier seems to be a practical measure. Thus, a required power capability of the amplifier is defined here as the required power rating of the amplifier with output impedance Z_S that ensures delivery of certain active power P_R to the load of impedance Z_L:

$$P_{\text{capab}} = \left| \frac{Z_L + Z_S}{\text{Re}\{Z_L\}} \right| P_R \tag{3}$$

Although the active power which is consumed by the actuator provides the most physical understanding of the power transduction process, the power capability of a driving source with a fixed impedance is a more practical measure indicating how powerful the amplifier needs to be. The interface shear stress generated by the piezoelectric actuation is now presented with reference to those power quantities. Note that stress is not linearly related to power, therefore the dimension of the *quasi*-transfer functions shown below is stress per square root of electrical power. The piezoelectric actuator is assumed to be linear in all cases considered in this paper.

3.2.1 Infinite plate in plane strain (1D cross-section)

The plane strain model extends to infinity in the x-direction, so for calculation of absorbed power some arbitrary width of the plate has to be chosen. In the following the output of the computation is scaled to represent a 20 mm wide strip. For the calculation of P_{capab} it is assumed that the driving source output impedance is 50 Ω, which implies that the P_{capab} results represent a particular case that could be significantly different if the source impedance were changed.

Interface shear stress results with reference to electrical power are shown in Fig. 6a. Assuming the strength of the aluminium–glaze ice bond σ_b to be 1.5 MPa, the corresponding power requirements are presented and plotted in Fig. 6b.

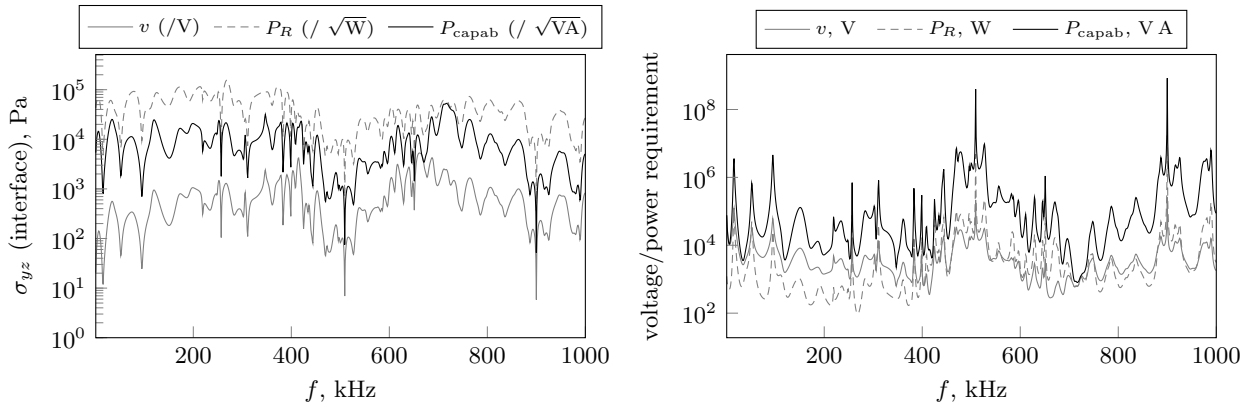

(a) interface shear stress as a function of electrical variables

(b) voltage and power requirements for de-icing assuming ice bond strength to be $\sigma_b = 1.5$ MPa

Figure 6: Interface shear stress at 0.1 m from the actuator and corresponding power requirements for de-icing in an infinite aluminium (2 mm) – glaze ice (2 mm) plate in plane strain equipped with a Noliac NCE40 2 mm thick and 5 cm long actuator; powers are scaled to a 20 mm wide strip.

The figures indicated by Fig. 6b appear to be practically non-realisable. From the active power perspective the best point is at 268 kHz, requiring 94 W of power to be consumed by the actuator for inducing debonding. If only a 50 Ω driving source is available, one would require its power capability to be higher than a few kilowatts which may put the practicability of the approach in question.

However, two additional aspects need to be taken into account. Firstly, the shear strength bond used in this paper is obtained statically and is expected to be higher than the dynamic bond strength. Secondly, the power capability is calculated for a 50 Ω source only (the typical off-the shelf characteristics). A dedicated system could have different output impedance adjusted to match the structural configuration, which can possibly lower the P_{capab} indications.

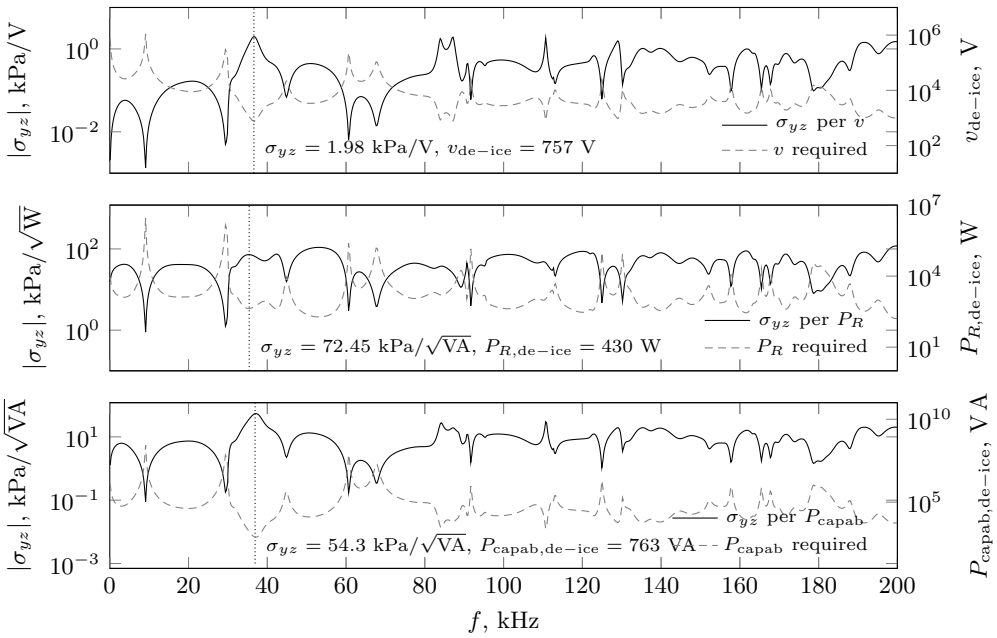

Figure 7: Interface shear stress per applied voltage and per square root of power quantities considered before for the beam as used in the experiment covered with 3 mm layer of glaze ice. On the secondary y axis, the voltage/power requirement is presented, assuming the ice bond braking stress to be $\sigma_b = 1.5$ MPa.

3.2.2 Infinite beam-like waveguide as used in the experiment (2D cross-section)

Attention is now drawn to a structural waveguide with a rectangular cross-section equipped with a 0.076 m and 2.2 mm thick Noliac NCE40 actuator (as used in the later experiment). The beam is covered over its whole length with a 3 mm thick glaze ice layer. The results showing the interface shear stress as a function of the applied voltage and the square root of electrical power are given in Fig. 7. On the secondary y-axes the voltage/power requirements for achieving delamination at the steel–glaze ice interface are depicted (assuming the bond strength σ_b to be 1.5 MPa). Additionally, the values near the across-width resonance of the PZT-covered section are specified.

A waveguide with a 2D cross-section benefits from higher order waves that are associated with across-width resonances of the cross-section. These are not available under the plane strain assumption and they give a rise to the interface shear stress. The higher-order wave in the PZT-covered section cuts off at around 36 kHz and is associated with a resonance of the actuator, providing the optimal power transfer between the electrical driving system and the structural waveguide. At that frequency the transverse shear stress at the interface with respect to P_{capab} reaches its maximum.

The respective power requirements shown in Fig. 7 are high and not directly acceptable from a practical perspective. However, it is worth keeping in mind that the ice bond strength (static) reported in the literature is not consistent among the authors and varies from 0.1 to 1.6 MPa. Moreover, the dynamic deformation is expected to break the bond easier, but unfortunately no results on the dynamic strength of the bond are known to the authors. If then the actual strength of the bond is two times smaller than the assumed $\sigma_b = 1.5$ MPa, the power requirements drops by a factor of four.

One also needs to bear in mind that the examples presented in this section refer to the worst case scenarios, i.e. when no end reflections are present and to debonding is to be induced only by a propagating wave. It is also clear that the interface stress values are very structure-specific. The examples chosen in this paper aim to demonstrate the capabilities of the developed wave model for predicting interface stress resulting from piezoelectric actuation. They give some indication of the realistic power requirements for specific structures but these requirements should not be generalised.

4. EXPERIMENT

In this final section we present an experiment in which the effectiveness of piezo-actuated structural waves in delaminating surface accretions is demonstrated. Focusing the interest on the effect of propagating waves only, we endeavoured to emulate anechoic boundary conditions at the ends of a beam-like waveguide. The ends of the beam were placed in boxes filled with sand in such a way that the thickness of the sand cover was gradually increased to ensure a smooth change in the mechanical impedance of the boundary and minimise any reflections.

4.1 Experimental setup and accretion material

The experimental setup is shown schematically in Fig. 8 and the details of the structural configuration in Fig. 9. The actuator was powered by an RF amplifier from Electronics & Innovation Ltd. (1020L) driven by the signal from a TTi TGA1240 arbitrary waveform generator. The generator output impedance can be set to 50 Ω in order to match the 1020L amplifier input impedance. The amplifier is equipped with an LCD display on which the forward and reflected power readings are shown.

The piezoelectric excitation aimed at removing surface patches made of plaster. We chose to use plaster as a material representing accretion as it is known to be brittle and of Young's modulus similar to ice accretions (see Fig. 10a). The commonly reported properties of ice are: Young's modulus – from 2.5 to 8.3 GPa, density – from 600 to 900 $\mathrm{kg\,m^{-3}}$.[23] These numbers indicate that plaster can be a good alternative to ice for experiments. Choosing plaster enabled circumventing the difficulties associated with producing and handling ice, while keeping similar material characteristics in place.

The shear adhesion strength of plaster was measured using a simple lap shear test to provide a reference for measurements. The breaking shear stress results are shown in Fig. 10b. Two different plaster mixes were tested: samples 1-10 as in Fig. 10b were made of 70% plaster mix (percentage of dry plaster mass), and samples 11-13 were made of 60% mix. For all cases the adhesion strength of plaster to aluminium is within the range between 0.142 and 0.366 MPa. No significant effect of changing the mixing ratio was observed. The overall variability

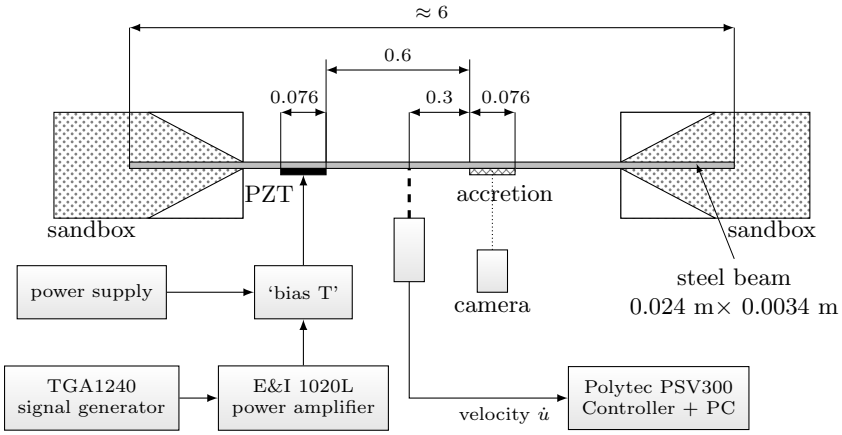

Figure 8: Experimental setup for the delamination attempt.

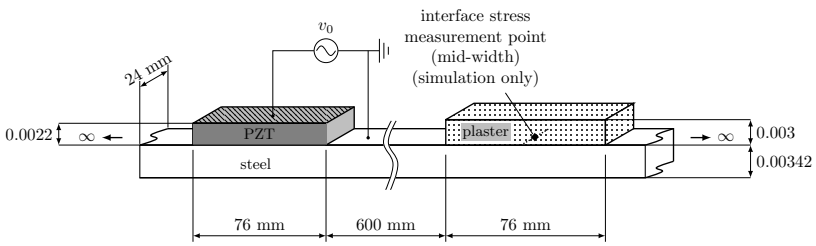

Figure 9: Structural configuration for simulations of interface shear stress in a beam-like waveguide covered with a plaster patch.

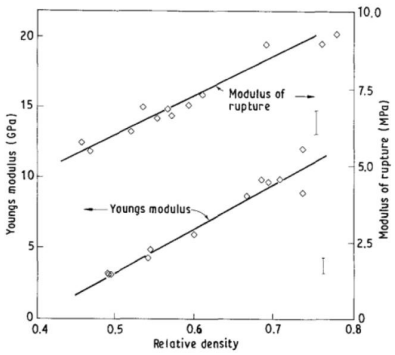

(a) Young's modulus of plaster.[24]

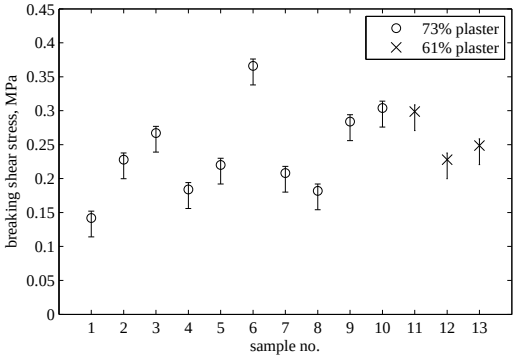

(b) Shear adhesion strength of the plaster-aluminium bond: experimental results.

Figure 10: Young's modulus of plaster and plaster adhesion strength results.

of the properties of patches due to mixing and forming process is higher than the supposed effect of increasing water content. Although high variability corresponds well to the real-type accretion scenarios, it is difficult to quantify using simple tests and makes the procedure more complicated. The results presented in Fig. 10b are found sufficient for the purpose of providing a reference for delamination experiments.

4.2 Simulated interface shear stress in a plaster-covered beam

The experiment is first performed numerically. The interface shear stress induced by the PZT actuator is simulated using the proposed computational approach. Plaster is treated as an isotropic material. The properties of the plaster are in general unknown and not measured here. Instead, they are assumed as follows: $E = 3$ GPa, $\rho = 1000\ \mathrm{kg\,m^{-3}}$, $\nu = 0.351$ and $\eta = 0.01$. The geometry and structural configuration for the considered case are shown in Fig. 9. For reference purposes the interface shear stress for a waveguide fully covered with plaster is also computed (with plaster layer on the surface opposite to the PZT).

Simulation results for interface shear stress with respect to different power quantities are shown in Fig. 11a. Up to around 60 kHz a similar level of interface shear stress is achieved for both partially and fully covered cases. It is expected that at low ultrasonic frequencies the frequency dependent characteristic impedance of the accretion is considerably smaller that that of the host beam, therefore the waves pass through the accreted region almost unchanged. At higher frequencies, wave scattering at the boundaries of the patch plays a more significant role and makes the overall response more complex. Given the available equipment, the interest is confined to frequencies below 80 kHz. This also aids physical insight into the phenomenon as only a few waves are present.

The maximum achievable stress if referred to the driving source power capability in the lower part of the frequency range in Fig. 11a is associated with the first higher-order wave (across-width bending) that cuts off in the PZT covered section around 36 kHz. The corresponding values for all chosen power reference quantities around that peak are listed in Fig. 11a. The frequency of the optimal electrical power transfer between the amplifier and the actuator is dictated by the electrical impedance of the actuator, which experiences a dip close the aforementioned cut-off frequency.

The power requirements for delaminating plaster are presented in Fig. 11b. As a representative value for generated interface shear stress, σ_{yz} at the middle of the width is chosen. The results indicate that the ultrasonic action can be successful if the actuator consumes 24 W of active power. It can be delivered to the actuator if a 50 Ω ultrasonic driving source is capable of producing 37 V A (and handle the impedance mismatch).

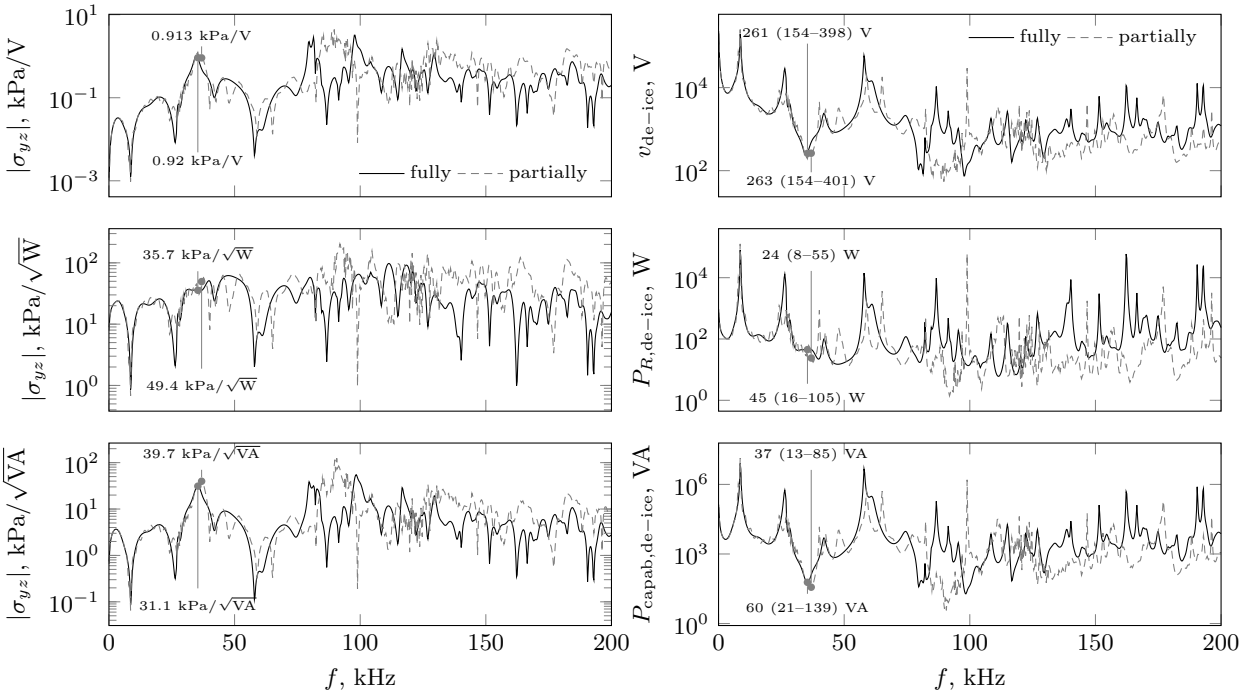

(a) interface shear stress

(b) voltage and power requirements Plaster bond strength as measured in the experiment – mean: 0.24 MPa (min: 0.142 MPa, max: 0.366 MPa.

Figure 11: Numerical results for interface shear stress and power requirements for delamination in a waveguide either fully or partially covered with 3 mm plaster accretion.

4.3 Procedure

In the experiment the output of the amplifier was shifted with a DC offset to ensure that the tensile stress within the actuator is minimised. Since PZT ceramics are much stronger in compression than in tension it is desirable to drive them predominantly in compression especially at high excitation levels to avoid tensile cracks.[10] This was achieved with a simple 'bias T' circuit which added the DC offset to the high amplitude signal and prevented feeding it back to the amplifier.

The following experimental procedure was adopted. Firstly, at a low level of excitation the optimum frequency was sought for around the 36 kHz resonance. The optimal frequency was identified based on the active power delivered to the actuator as indicated by the amplifier's display. After the frequency had been tuned, the driving power was increased up to the point when plaster patch shedding was observed. For reference purposes, the surface velocity at a point equidistant from the actuator and the accreted patch was measured using a laser vibrometer for one of the experimental runs.

4.3.1 Results

The delamination was attempted in a few different runs of which some conformed to the structural configuration showed in Fig. 9 and the others did not (e.g. more patches were placed on the beam). The results indicating the active (consumed) power at the instant of delamination are listed in Tab. 2, and illustrative video snapshots showing the patches shedding are presented in Fig. 12. Piezo-actuated structural waves were proven to be able to invoke delamination and remove the accretion.

After the patches had shed it was observed that some of them were only partially attached to the host beam, which made the debonding very difficult. Imperfect bond between the layers significantly diminishes the generated interface stress which results in higher power requirements. We also noted that wave absorption at

Table 2: Consumed power at the successful delamination attempts.

Run #	P_{FWD}	P_{RFD}	P_R	configuration
1	83 W	63 W	20 W @ 35.61 kHz	as in Fig. 9
2	52 W	32 W	20 W @ 35.32 kHz	as in Fig. 9
3	93 W	56 W	37 W	different from Fig. 9
4	130 W	81 W	49 W	different from Fig. 9
5	18 W	8 W	10 W	different from Fig. 9

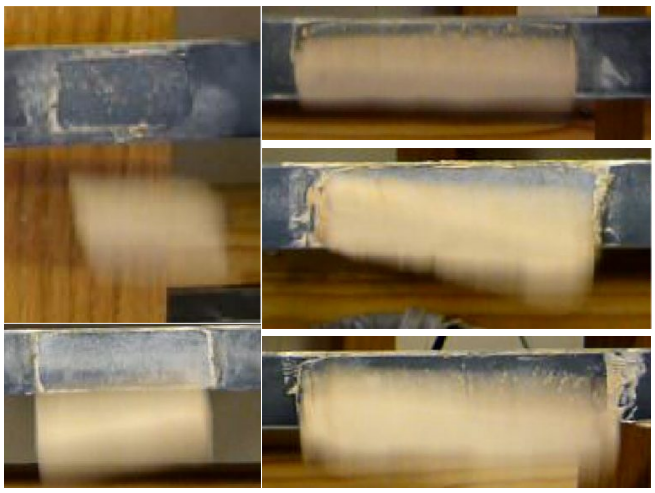

Figure 12: Video snapshots showing the plaster patches falling of the beam as a result of the ultrasonic actuation.

the boundaries was not ideal in the experimental rig, therefore the delamination experiment benefited from the effect of reflections albeit small in magnitude.

For the two runs for which the structural configuration was the same as in the simulations in Fig. 11b the active power consumption at the delamination was measured to be 20 W. The corresponding numerical simulation indicates a higher value of 24 W. Given the variability of the shear adhesion strength of plaster, these results seem to be in good agreement. However, it is noted that the properties of plaster assumed in the simulation were not rigorously measured and that the numerical results assume a perfect bond between the patch and the host structure.

In order to further verify the link between the model and the experimental arrangement, the surface velocity of the beam was monitored during the delamination in run 1. (see Tab. 2.) The time history corresponding to the instant when the patch shed is shown in Fig. 13a. The relevant numerical results computed using the developed wave model are presented in Fig. 13b.

During successful delamination attempts 20 W of active powered was consumed. Using the data from Fig. 13b one can calculate that if the actuator is driven with 20 W of active power the surface velocity is 191.0 mm/s. The observed surface velocity is 432.7 mm/s, which is more than twice the predicted value from simulation. This may be attributable to the residual reflections from the sandboxes which give rise to the response. If so, the interface shear stress generated by the 20 W ultrasonic actuation would be twice as high as predicted by the model.

At 20 W of active power the model predicts the shear stress of 0.16 MPa at the interface. If one follows the observation that response is doubled compared to the numerical prediction, the interface shear stress generated in the experiment is 0.32 MPa which is very close to the upper-bound values measured for plaster bond strength from Fig. 10b.

Given the aforementioned uncertainties in the experimental arrangement of which analysis falls outside of the scope of this paper, it is acknowledged that piezo-actuated ultrasonic waves were demonstrated to be capable

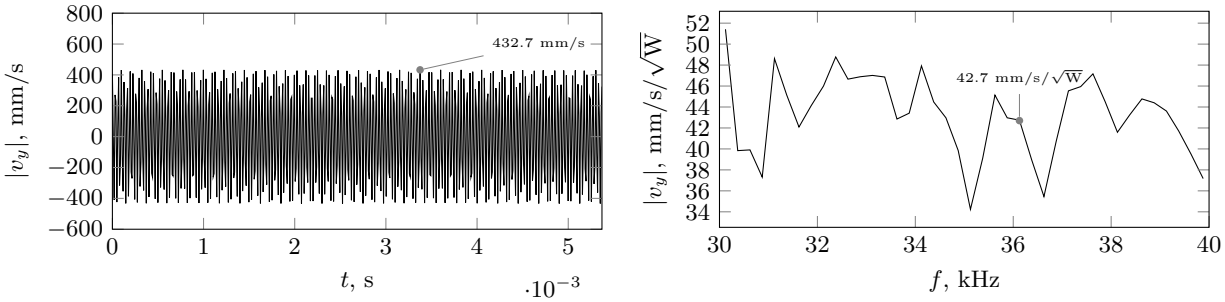

(a) recorded during the successful delamination attempt. (b) numerical results with respect to the active power.

Figure 13: Surface velocity at the middle of the width of the steel beam.

of removing surface accretion. The power requirements observed in the experimental demonstration were of an acceptable level and similar to those predicted by the numerical model (accounting for the differences explained above). This confirms that the modelling technique demonstrated in this paper can be useful for a class of problems requiring computation of high-power (yet still linear) piezoelectric actuation. Moreover, it shows the potential of high-frequency structural waves for delaminating unwanted build-ups.

5. CONCLUSIONS

In this paper the capability of piezo-excited structural waves for delaminating surface accretion was discussed. The numerical part focused on calculating the interface shear stress generated by piezoelectric actuation and referring it to the electrical power requirements. The transfer functions and *quasi*-transfer functions between the interface shear stress and voltage and power were presented and contributions from particular wave modes separated.

The numerical calculations were performed using a wave model based on the SAFE method (including a piezoelectric SAFE element) and the analytical wave approach. The model includes full dynamics of the actuator and its mutual interaction with the structure as well as is capable of analysing waveguides of an arbitrary cross-section. These features proved vital for modelling this application.

The paper concluded with the experimental demonstration of the concept. Accretions from plaster were attached to the beam with emulated anechoic terminations. Piezo-actuated structural waves were proven capable of removing the accretions. For some of the cases the numerical counterpart was simulated. The computed power requirements corresponded reasonably well with the power consumption associated with delamination observed during the experiment.

ACKNOWLEDGMENTS

This research is possible thanks to the University of Southampton Postgraduate Research Studentship Programme. Financial support of Structural Funds in the Operational Programme - Innovative Economy (IE OP) financed from the European Regional Development Fund - Project "Modern material technologies in aerospace industry", Nr POIG.01.01.02-00-015/08-00 is gratefully acknowledged.

REFERENCES

[1] Adachi, K., Saiki, K., and Sato, H., "Supression of frosting on a metal surface using ultrasonic vibrations," *Proceedings of the IEEE Ultrasonics Symposium* , 759–762 (1998).

[2] Ramanathan, S., *An Investigation on the Deicing of Helicopter Blades Using Shear Horizontal Guided Waves*, PhD thesis, Pennsylvania State University. Department of Engineering Science and Mechanics (2005).

[3] Seppings, R. A., *Investigation of Ice Removal From Cooled Metal Surfaces*, PhD thesis, Imperial College, Mechanical Engineering Department, University of London (Oct. 2005).

[4] Palacios, J., "Ultrasonic shear and Lamb wave interface stress for helicopter rotor de-icing purposes," in [*47th AIAA Structural Dynamics & Materials, Newport, Rhode Island*], (2006).

[5] Palacios, J., Smith, E., Zhu, Y., and Rose, J., "Global ultrasonic shear wave anti-icing actuator for helicopter blades," in [*American Helicopter Society 64th Annual Forum, Montreal, Canada*], (2007).

[6] Palacios, J., *Design, Fabrication and Testing of an Ultrasonic De-icing System for Helicopter Blades*, PhD thesis, Pennsylvania State University. Department of Aerospace Engineering (2008).

[7] Palacios, J. and Smith, E., "Invetsigation of an ultrasonic ice protection system for helicopter rotor blades," in [*American Helicopter Society 64th Annual Forum, Montreal, Canada*], (2008).

[8] Palacios, J., Smith, E., Rose, J., and Royer, R., "Instantaneous de-icing of freezer ice via ultrasonic actuation," *AIAA Journal* **49**(6), 1158–1167 (2011).

[9] Palacios, J., Smith, E., Rose, J., and Royer, R., "Ultrasonic de-icing of wind-tunnel impact icing," *Journal of Aircraft* **48**(3), 1020–1027 (2011).

[10] Overmeyer, A., Palacios, J., Smith, E., and Royer, R., "Rotating testing of a low-power, non-thermal ultrasonic de-icing system for helicopter rotor blades," in [*SAE 2011 International Conference on Aircraft and Engine Icing and Ground Deicing, Chicago, Illinois*], (June 2011).

[11] Zhu, Y., *Structural Tailoring and Actuation Studies for Low Power Ultrasonic De-icing of Aluminium and Composite Plates*, PhD thesis, Pennsylvania State University. Department of Engineering Science and Mechanics (2010).

[12] DiPlacido, N., Soltis, J., Smith, E., and Palacios, J., "Enhancement of ultrasonic de-icing via transient excitation," in [*Proceedings of the 2nd Asian/Australian Rotorcraft Forum and The 4th International Basic Research Conference on Rotorcraft Technology*], (Sept. 2013).

[13] Li, D. and Chen, Z., "Experimental study on instantaneously shedding frozen water droplets from cold vertical surface by ultrasonic vibration," *Experimental Thermal and Fluid Science* **53**, 17–25 (Feb. 2014).

[14] Kalkowski, M., Rustighi, E., and Waters, T., "Modelling piezoelectric excitation in waveguides using the semi-analytical finite element method," *Computers & Structures* **(under review)** (2014).

[15] Kalkowski, M., *Piezo-actuated structural waves for delaminating surface accretions*, PhD thesis, University of Southampton. Faculty of Engineering and the Environment. Institute of Sound and Vibration Research (January 2015).

[16] Hayashi, T., Song, W.-J., and Rose, J. L., "Guided wave dispersion curves for a bar with an arbitrary cross-section, a rod and rail example," *Ultrasonics* **41**, 175–183 (May 2003).

[17] Damljanovic, V. and Weaver, R. L., "Forced response of a cylindrical waveguide with simulation of the wavenumber extraction problem," *The Journal of the Acoustical Society of America* **115**(4), 1582 (2004).

[18] Bartoli, I., Marzani, A., Lanza di Scalea, F., and Viola, E., "Modeling wave propagation in damped waveguides of arbitrary cross-section," *Journal of Sound and Vibration* **295**, 685–707 (Aug. 2006).

[19] Harland, N., Mace, B., and Jones, R., "Wave propagation, reflection and transmission in tunable fluid-filled beams," *Journal of Sound and Vibration* **241**, 735–754 (Apr. 2001).

[20] Waki, Y., *On the application of finite element analysis to wave motion in one-dimensional waveguides*, PhD thesis, University of Southampton (2007).

[21] Huang, G., Song, F., and Wang, X., "Quantitative modeling of coupled piezo-elastodynamic behavior of piezoelectric actuators bonded to an elastic medium for structural health monitoring: A review," *Sensors* **10**, 3681–3702 (Apr. 2010).

[22] Eskandarian, M., *Ice shedding from overhead electrical lines by mechanical breaking*, PhD thesis, University of Quebec (September 2005).

[23] Gao, H. and Rose, J., "Ice detection and classification on an aircraft wing with ultrasonic shear horizontal guided waves," *IEEE Transactions on Ultrasonics, Ferroelectrics, and Frequency Control* **56**(2), 334–344 (2009).

[24] Vekinis, G., Ashby, M., and Beaumont, P., "Plaster of paris as a model material for brittle porous solids," *Journal of Materials Science* **28**(12), 3221–3227 (1993).